

Multiple Transitions and Disease Localization in Multilayer Networks

Guilherme Ferraz de Arruda,^{1,2} Emanuele Cozzo,^{2,3} Tiago P. Peixoto,^{4,5} Francisco A. Rodrigues,^{1,*} and Yamir Moreno^{2,3,6,†}

¹*Departamento de Matemática Aplicada e Estatística, Instituto de Ciências Matemáticas e de Computação, Universidade de São Paulo - Campus de São Carlos, Caixa Postal 668, 13560-970 São Carlos, SP, Brazil.*

²*Institute for Biocomputation and Physics of Complex Systems (BIFI), University of Zaragoza, Zaragoza 50009, Spain*

³*Department of Theoretical Physics, University of Zaragoza, Zaragoza 50009, Spain*

⁴*Institut für Theoretische Physik, Universität Bremen, Hochschulring 18, D-28359 Bremen, Germany*

⁵*ISI Foundation, Turin, Italy*

⁶*Complex Networks and Systems Lagrange Lab, Institute for Scientific Interchange, Turin, Italy*

We present a continuous formulation of epidemic spreading on multilayer networks using a tensorial representation, extending the models of monoplex networks to this context. We derive analytical expressions for the epidemic threshold of the SIS and SIR dynamics, as well as upper and lower bounds for the disease prevalence in the steady state for the SIS scenario. Using the quasi-stationary state (QS) method we numerically show the existence of disease localization and the emergence of two or more phase transitions, which are characterized analytically and numerically through the inverse participation ratio. Furthermore, when mapping the critical dynamics to an eigenvalue problem, we observe a characteristic transition in the eigenvalue spectra of the supra-contact tensor as a function of the ratio of two spreading rates: If the rate at which the disease spreads within a layer is comparable to the spreading rate across layers, the individual spectra of each layer merge with the coupling between layers. The formalism introduced here provides a unifying mathematical approach to disease contagion in multiplex systems opening new possibilities for the study of spreading processes. Finally, our findings show the importance of considering the multilayer nature of many real systems, as this interdependency usually gives raise to new phenomenology.

I. INTRODUCTION

Epidemic like spreading processes are paradigmatic, as they can describe not only the temporal unfolding and evolution of diseases, but also of ideas, information and rumors in fields as diverse as biological, information and social sciences [1]. Due to their fundamental nature and simplicity, two particular models have received special attention by the scientific community, the Susceptible-Infected-Susceptible (SIS) and the Susceptible-Infected-Recovered (SIR). In both models, an infected individual spreads the disease to its neighbors at a given (spreading) rate and infected individuals recovers at some other rate. The difference between both scenarios is that in the SIS case, once recovered, infected individuals are considered to be able to catch the disease again, and therefore, they go back to the susceptible state. On the contrary, in the SIR model, recovered individuals are supposed to acquire permanent immunity -hence why they are also referred to as removed- and they do not play any active role in the spreading process anymore. There are many other variations of these two models, including more realistic and intricate compartmental models [1], however, these two schemes are sufficient to capture the main phenomenology of disease dynamics -and many other con-

tagion like processes-, including the onset of epidemics, while remaining simple.

Originally, the modeling of diseases was confined to homogeneous systems, where any pair of individuals have the same probability of being in contact [2, 3]. As shown since early 2000's, this is not in general a realistic assumption, and therefore, previous results were re-examined considering non-trivial patterns among individuals, such as power law degree distributions [4-6]. In [7], the authors presented the heterogeneous mean-field approach (HMF), showing that the epidemic threshold tends to zero in the thermodynamic limit on scale-free networks. This observation that the network structure radically influences basic but fundamental pillars of epidemiology - like the epidemic threshold and immunization protocols- changed completely our previous understanding of how disease outbreaks should be modeled, placing the focus of attention not only into new ways to model disease dynamics, but also to the incorporation of real contact patterns into the dynamical settings [3, 8-11].

Since then, many computational and theoretical frameworks have been proposed, which undoubtedly had made the modeling of disease contagion an active area of research and have provided new phenomenological insights to, and accurate methods for the study of real outbreaks. For instance, instead of the HMF approach, one can adopt the quenched mean field (QMF) method, where a specific network is fixed and the dynamics is modeled in terms of nodal probabilities [12, 13]. The results obtained with the latter approach show that the epidemic

*Electronic address: francisco@icmc.usp.br

†Electronic address: yamir.moreno@gmail.com

threshold depends on the inverse of the leading eigenvalue of the adjacency matrix [12, 13] -a similar result was also obtained using a discrete Markov Chain Approach [14]. Other scenarios explored recently include the case of temporal networks [15, 16], competing and interacting diseases [17–23] as well as the inclusion of human behavioral responses [24–26].

However, the vast majority of the works so far deal with single-layered networks, despite the fact that many real systems exhibits a large degree of interconnectivity and hence should be modeled as layers of coupled networks. Such systems represent multimodal, different categorical or temporal interactions, as for instance social relations, the ecosystem formed by different online social networks or modern transportation systems [27]. With this in mind, in Ref. [28], the authors showed that disregarding the multilayer structure can lead to misleading conclusions, missing fundamental aspects of the critical dynamics of spreading like processes. Such findings reinforce the importance of a more detailed investigation of contagion processes on multilayer networks. In this work, we develop a theoretical and computational framework for the analysis of disease spreading, generalizing the results of Ref. [13] to multilayer networks. In doing so, we provide a continuous counterpart to the model presented in [28] in terms of the tensorial notation introduced in [29]. The methodology introduce here allows for several new results: first, we are able to write down in a compact form the equations describing the disease dynamics in a multilayer system. Secondly, we derive the corresponding epidemic thresholds for the SIS and SIR case as well as establish bounds for the prevalence of the disease in the SIS scenario. We also identify previously unnoticed multiple transitions and disease localization, which are traced back to the very topological nature of the system and described in terms of the eigenvalue spectra of the supra-contact tensor and the localization of eigenstates.

The rest of the paper is organized as follows: we first formally define a multilayer network, introducing the tensorial notation. Next we derive the equations describing the dynamics of the disease for the SIS scheme, calculating the upper and lower bounds for the prevalence of the disease in the steady state, followed by the analytical expression for the epidemic threshold -which is also derived for the SIR model. Furthermore, we use the results in [30] to define some constraints on the critical point. In addition, we explore the notion of localization of eigenstates, formerly applied on epidemic spreading in [31], in order to inspect multiple phase transitions. Finally, we also present results from extensive numerical simulations considering multiplex networks with scale-free and scale-rich structures, computing their respective epidemic thresholds. Finally, we present our conclusions in the last Section.

II. CONTINUOUS FORMULATION FOR MULTILAYER EPIDEMIC SPREADING

A. Tensorial representation

We use here the tensorial representation, formerly presented in [29]. We also adopt the Einstein summation convention, in order to have more compact equations: If two indices are repeated, where one is a superscript and the other a subscript, then such operation implies a summation. Aside from that, the result is a tensor whose rank lowers by 2. For instance, $A_\beta^\alpha A_\alpha^\gamma = \sum_\alpha A_\beta^\alpha A_\alpha^\gamma$. In our notation we use greek letters to indicate the components of a tensor. In addition, we use tilde ($\tilde{\cdot}$) to denote the components related to the layers, with dimension m , while the components without tilde have dimension n and are related to the nodes.

A multilayer network is represented as the fourth-order adjacency tensor $M \in \mathbb{R}^{n \times n \times m \times m}$ [29]

$$\begin{aligned} M_{\beta\gamma}^{\alpha\delta} &= \sum_{\tilde{h}, \tilde{k}=1}^m C_\beta^\alpha(\tilde{h}\tilde{k}) E_\gamma^\delta(\tilde{h}\tilde{k}) = \\ &= \sum_{\tilde{h}, \tilde{k}=1}^m \sum_{i,j=1}^n w_{ij}(\tilde{h}\tilde{k}) \mathcal{E}_{\beta\gamma}^{\alpha\delta}(ij\tilde{h}\tilde{k}), \end{aligned} \quad (1)$$

where $E_\delta^\gamma(\tilde{h}\tilde{k}) \in \mathbb{R}^{m \times m}$ and $\mathcal{E}_{\beta\gamma}^{\alpha\delta}(ij\tilde{h}\tilde{k}) \in \mathbb{R}^{n \times n \times m \times m}$ indicate the tensor in its respective canonical basis. Observe that we can extract one layer by projecting the tensor $M_{\beta\gamma}^{\alpha\delta}$ to the canonical tensor $E_\delta^\gamma(\tilde{r}\tilde{r})$. Formally, from [29] we have

$$M_{\beta\gamma}^{\alpha\delta} E_\delta^\gamma(\tilde{r}\tilde{r}) = C_\beta^\alpha(\tilde{r}\tilde{r}) = A_\beta^\alpha(\tilde{r}), \quad (2)$$

where $\tilde{r} \in \{1, 2, \dots, m\}$ is the selected layer and $A_\beta^\alpha(\tilde{r})$ is the adjacency matrix (rank-2 tensor). Moreover, aiming at having more compact and clear equations we define the all-one tensors $u_\alpha \in \mathbb{R}^n$ and $U^{\beta\delta} \in \mathbb{R}^{n \times m}$. Here, we restrict our analysis to multilayer networks with a diagonal coupling [27]. In other words, each node can have at most one counterpart on the other layers. In addition, for simplicity, we focus on unweighted and undirected connected networks, in which there is a path from each node to all other nodes.

Besides the adjacency tensor, the network of layers [30] also characterizes the topology of the system. In this reduced network representation, each node represents one layer and the edges between them codify the number of edges connecting those two layers. Formally we have,

$$\Psi_\delta^\gamma = M_{\beta\delta}^{\alpha\gamma} U_\alpha^\beta, \quad (3)$$

where $\Psi_\delta^\gamma \in \mathbb{R}^{m \times m}$. Note that such a network presents self-loops, which are weighted by the number of edges on the layer. Additionally, since we assume that the layers have the same number of nodes, the edges of the network of layers have weights equal to the number of nodes n .

Another important reduction of the multilayer network is the so-called projection [29]. Such network aggregates all the information into one layer, including self-loops that stand for the number of layers in which a node appears. Mathematically, we have

$$P_{\beta}^{\alpha} = M_{\beta\tilde{\gamma}}^{\alpha\tilde{\delta}} U_{\tilde{\delta}}^{\tilde{\gamma}}, \quad (4)$$

where $P_{\beta}^{\alpha} \in \mathbb{R}^{n \times n}$.

B. The Susceptible-Infected-Susceptible (SIS) model

Next, we define the SIS disease dynamics, which is modeled as follows. We associate a Poisson process to each of the elementary dynamical transitions: intra and inter layer spreading and the recovery from the infected state. The first two processes are associated to the edges of the graph and are characterized by the parameters λ and η , respectively. The latter transition is modeled in the node, also via a Poisson process with parameter δ . Using the tensorial notation defined above, the equations describing the systems dynamics read as

$$\frac{dX_{\beta\tilde{\delta}}}{dt} = -\mu X_{\beta\tilde{\delta}} + \left(1 - X_{\beta\tilde{\delta}}\right) \lambda \mathcal{R}_{\beta\tilde{\delta}}^{\alpha\tilde{\gamma}}(\lambda, \eta) X_{\alpha\tilde{\gamma}}, \quad (5)$$

where the supra contact tensor is defined as

$$\mathcal{R}_{\beta\tilde{\delta}}^{\alpha\tilde{\gamma}}(\lambda, \eta) = M_{\beta\tilde{\sigma}}^{\alpha\tilde{\eta}} E_{\tilde{\eta}}^{\tilde{\sigma}}(\tilde{\gamma}\tilde{\delta})\delta_{\tilde{\delta}}^{\tilde{\gamma}} + \frac{\eta}{\lambda} M_{\beta\tilde{\sigma}}^{\alpha\tilde{\eta}} E_{\tilde{\eta}}^{\tilde{\sigma}}(\tilde{\gamma}\tilde{\delta})(U_{\tilde{\delta}}^{\tilde{\gamma}} - \delta_{\tilde{\delta}}^{\tilde{\gamma}}), \quad (6)$$

which encodes the contacts. It has a similar role as the matrix R in [28]. Important enough, note that we have implicitly assumed that the random variables $X_{\beta\tilde{\delta}}$ are independent. Formally, if the state variable $S_{\beta\tilde{\delta}}$ is such that $S_{\beta\tilde{\delta}} = 1$ when the node β on layer $\tilde{\delta}$ is an spreader and $S_{\beta\tilde{\delta}} = 0$ otherwise, then $P[S_{\beta\tilde{\delta}} = 1] = X_{\beta\tilde{\delta}}$. In this way, the independence of random variables implies that $P[S_{\beta\tilde{\delta}} = 1, S_{\alpha\tilde{\gamma}} = 1] = P[S_{\beta\tilde{\delta}} = 1]P[S_{\alpha\tilde{\gamma}} = 1] = X_{\beta\tilde{\delta}}X_{\alpha\tilde{\gamma}}$. Cator and Van Mieghem [32] proved rigorously that the states of any two nodes in the SIS model are non-negatively correlated for all finite graphs. This result can be easily extended to our case, since we are considering constant rates and Markovian processes. Due to the positive contribution of the infected nodes we have $P[S_{\beta\tilde{\delta}} = 1 | S_{\alpha\tilde{\gamma}} = 1] \geq P[S_{\beta\tilde{\delta}} = 1]$, implying that the model is always overestimated. A similar conclusion was also obtained in [13] for the monolayer model.

Moreover, we define the macro-state variable as

$$\rho = \frac{1}{nm} X_{\beta\tilde{\delta}} U^{\beta\tilde{\delta}}, \quad (7)$$

which is the average of the individual probabilities. Note that the steady state is not an absorbing state in the Markov sense, since there is a set of possible states where the system remains trapped and there is a stochastic variation over time. Moreover, there are many different configurations for which the fraction of infected nodes is the

same. More formally, there is a set of states above the threshold which have finite probability larger than zero, configuring a meta-state. The only absorbing state of this set of equations is thus the disease-free state, since when it is reached the (micro and macro) dynamics stops.

1. Upper and lower bounds for the steady-state

Let us first obtain some bounds for the epidemic incidence considering the steady state, where $\frac{dX_{\beta\tilde{\delta}}}{dt} = 0$. For a monolayer system those bounds were calculated in [13]. We consider a multilayer network without self loops and denote the steady state of each node as $X_{\beta\tilde{\delta}}^{\infty}$.

Then, imposing $\frac{dX_{\beta\tilde{\delta}}}{dt} = 0$ to Eq. 5 we have

$$X_{\beta\tilde{\delta}}^{\infty} = \frac{\lambda \mathcal{R}_{\beta\tilde{\delta}}^{\alpha\tilde{\gamma}}(\lambda, \eta) X_{\alpha\tilde{\gamma}}^{\infty}}{\lambda \mathcal{R}_{\beta\tilde{\delta}}^{\alpha\tilde{\gamma}}(\lambda, \eta) X_{\alpha\tilde{\gamma}}^{\infty} + \mu} = 1 - \frac{1}{\frac{\lambda}{\mu} \mathcal{R}_{\beta\tilde{\delta}}^{\alpha\tilde{\gamma}}(\lambda, \eta) X_{\alpha\tilde{\gamma}}^{\infty} + 1}. \quad (8)$$

The value of $X_{\beta\tilde{\delta}}^{\infty}$ is then obtained by iterating the above equation from an initial value, until convergence. Upper and lower bounds can be obtained by considering only the first iteration of Eq. 8. For the upper bound we have

$$X_{\beta\tilde{\delta}}^{\infty} \leq 1 - \frac{1}{\left(\frac{\lambda}{\mu}\right) d_{\beta\tilde{\delta}} + 1}. \quad (9)$$

where

$$\begin{aligned} d_{\beta\tilde{\delta}} &= \mathcal{R}_{\beta\tilde{\delta}}^{\alpha\tilde{\gamma}}(\lambda, \eta) U_{\alpha\tilde{\gamma}} = \\ &= M_{\beta\tilde{\gamma}}^{\alpha\tilde{\xi}} E_{\tilde{\xi}}^{\tilde{\gamma}}(\tilde{\delta}\tilde{\delta}) u_{\alpha} + \frac{\eta}{\lambda} M_{\nu\tilde{\delta}}^{\xi\tilde{\gamma}} E_{\xi}^{\nu}(\beta\beta) u_{\tilde{\gamma}}. \end{aligned} \quad (10)$$

As can be noticed, there are two different contributions to the upper bound coming from intra and inter-layers connectivity. Both of them tend to increase the probability of a node being infected. Furthermore, the higher is the degree, the higher is this upper bound. On the other hand, for the lower bound, let us denote $\text{Min}\{X_{\beta\tilde{\delta}}^{\infty}\} = X^{\text{min}}$. Then, substituting X^{min} in Eq. 8 we have

$$X^{\text{min}} \geq 1 - \frac{1}{\frac{\lambda}{\mu} \mathcal{R}_{\beta\tilde{\delta}}^{\alpha\tilde{\gamma}}(\lambda, \eta) U_{\alpha\tilde{\gamma}} X^{\text{min}} + 1}. \quad (11)$$

Denoting $\text{Min}\{d_{\beta\tilde{\delta}}\} = d^{\text{min}}$, we obtain

$$X^{\text{min}} \geq 1 - \frac{1}{\left(\frac{\lambda}{\mu}\right) d^{\text{min}}}, \quad (12)$$

which can be inserted into Eq. 8 to give,

$$X_{\beta\tilde{\delta}}^{\infty} \geq X^{\text{min}} \geq 1 - \frac{1}{1 + \frac{d_{\beta\tilde{\delta}}}{d^{\text{min}}} \left[\left(\frac{\lambda}{\mu}\right) d^{\text{min}} - 1\right]}. \quad (13)$$

Finally, combining Eqs. 9 and 13, the bounds of Eq. 5 are

$$1 - \frac{1}{1 + \frac{d_{\beta\bar{\delta}}}{d^{\min}} \left[\left(\frac{\lambda}{\mu} \right) d^{\min} - 1 \right]} \leq X_{\beta\bar{\delta}}^{\infty} \leq 1 - \frac{1}{\left(\frac{\lambda}{\mu} \right) d_{\beta\bar{\delta}} + 1}. \quad (14)$$

Note that the higher d^{\min} , the closer the lower and upper bounds. In the extreme case $\left(\frac{\lambda}{\mu} \right) \rightarrow \infty$ the bounds approach each other and all nodes tend to be infected. Phenomenologically, the latter parameter configuration models the limiting case of a SI-like scenario, where $\mu = 0$. In such a dynamical process all individuals are infected in the steady state.

2. Eigenvalue problem

As we will show below, the epidemic threshold is closely related to the leading eigenvalues of the supra-contact tensor. Here we describe the eigenvalue problem in general, and then in the following section we show the connection with the epidemic threshold.

The eigenvalue problem can be generalized to the case of a rank-4 tensor leading to

$$\mathcal{R}_{\beta\bar{\delta}}^{\alpha\bar{\gamma}} f_{\alpha\bar{\gamma}}(\Lambda) = \Lambda f_{\beta\bar{\delta}}(\Lambda), \quad (15)$$

where Λ is an eigenvalue and $f_{\beta\bar{\delta}}(\Lambda)$ is the corresponding eigentensor. In addition, we are assuming that the eigentensors form an orthonormal basis. Importantly, the supra-contact matrix, R , in [28] can be understood as a flattened version of the tensor $\mathcal{R}_{\beta\bar{\delta}}^{\alpha\bar{\gamma}}(\lambda, \eta)$. Consequently, all the results for R also apply to the tensor \mathcal{R} . As argued in [29], that supra-adjacency matrix corresponds to unique unfolding of the fourth-order tensor m yielding square matrices. Following this unique mapping we have the correspondence of the eigensystems. Here, we consider that the eigenvalues are ordered as $\Lambda_1 \geq \Lambda_2 \geq \dots \Lambda_{nm}$ and denote the individual layer eigenvalues as Λ_i^l .

3. The epidemic threshold

Assuming $\mu > 0$ and that the dynamics has reached the steady state, $\frac{dX_{\beta\bar{\delta}}}{dt} = 0$, we can write eq. 5 as

$$\frac{X_{\beta\bar{\delta}}^{\infty}}{1 - X_{\beta\bar{\delta}}^{\infty}} = \left(\frac{\lambda}{\mu} \right) \mathcal{R}_{\beta\bar{\delta}}^{\alpha\bar{\gamma}} X_{\alpha\bar{\gamma}}^{\infty}. \quad (16)$$

Expanding the left-hand term following the geometrical series, where $\frac{X_{\beta\bar{\delta}}^{\infty}}{1 - X_{\beta\bar{\delta}}^{\infty}} = \sum_{k=1}^{\infty} \left(X_{\beta\bar{\delta}}^{\infty} \right)^k$ for $X_{\beta\bar{\delta}}^{\infty} < 1$, we obtain

$$\left(\frac{\mu}{\lambda} \right) \sum_{k=1}^{\infty} \left(X_{\beta\bar{\delta}}^{\infty} \right)^k = \mathcal{R}_{\beta\bar{\delta}}^{\alpha\bar{\gamma}}(\lambda, \eta) X_{\alpha\bar{\gamma}}^{\infty}. \quad (17)$$

In addition, similarly to [13], suppose $X_{\beta\bar{\delta}}^{\infty} = \epsilon f_{\beta\bar{\delta}}$, where ϵ is an arbitrary small constant and $f_{\beta\bar{\delta}} \geq 0$. Substituting in eq. 17 and dividing by ϵ we have

$$\mathcal{R}_{\beta\bar{\delta}}^{\alpha\bar{\gamma}}(\lambda, \eta) f_{\alpha\bar{\gamma}} = \left(\frac{\mu}{\lambda} \right) f_{\beta\bar{\delta}} + \epsilon \left(\frac{\mu}{\lambda} \right) \left(f_{\beta\bar{\delta}} \right)^2 + \mathcal{O}(\epsilon^2). \quad (18)$$

Considering a sufficiently small $\epsilon > 0$ this expression reduces to the eigentensor equation

$$\mathcal{R}_{\beta\bar{\delta}}^{\alpha\bar{\gamma}}(\lambda, \eta) f_{\alpha\bar{\gamma}} = \left(\frac{\mu}{\lambda} \right) f_{\beta\bar{\delta}}, \quad (19)$$

leading to the critical point

$$\left(\frac{\mu}{\lambda} \right)_c = \Lambda_1, \quad (20)$$

where Λ_1 is the largest eigenvalue of \mathcal{R} , which is the same as the largest eigenvalue of R in [28]. Moreover, if $\eta M_{\nu\bar{\delta}}^{\xi\bar{\gamma}} E_{\xi}^{\nu}(\beta\bar{\delta}) \ll \lambda M_{\beta\bar{\gamma}}^{\alpha\bar{\xi}} E_{\xi}^{\bar{\gamma}}(\bar{\delta}\bar{\delta})$, the threshold of the system is dominated by the individual layer behavior and the epidemic threshold is approximated to that of a SIS model on monolayers, when considering the union of m disjoint networks. Consequently, the epidemic threshold is determined by the largest eigenvalue, considering all layers. The same conclusion was reached in [28] using perturbation theory on the supra-contact matrix.

C. The Susceptible-Infected-Recovered (SIR) Model

Aside from the SIS epidemic model, we can also consider the SIR model. The recovered and susceptible states are denoted here as $Y_{\beta\bar{\delta}}$ and $Z_{\beta\bar{\delta}}$, respectively. Using a similar notation as in the latter section and associating Poisson processes to nodes and edges, we have the dynamical set of equations

$$\begin{aligned} \frac{dX_{\beta\bar{\delta}}}{dt} &= -\mu X_{\beta\bar{\delta}} + Z_{\beta\bar{\delta}} \lambda \mathcal{R}_{\beta\bar{\delta}}^{\alpha\bar{\gamma}}(\lambda, \eta) X_{\alpha\bar{\gamma}} \\ \frac{dY_{\beta\bar{\delta}}}{dt} &= \mu X_{\beta\bar{\delta}} \\ \frac{dZ_{\beta\bar{\delta}}}{dt} &= -Z_{\beta\bar{\delta}} \lambda \mathcal{R}_{\beta\bar{\delta}}^{\alpha\bar{\gamma}}(\lambda, \eta) X_{\alpha\bar{\gamma}}. \end{aligned} \quad (21)$$

Note that the Poisson processes on the nodes model the recovering, whereas on the edges, model the spreading.

1. Epidemic threshold

Since there is no dynamic steady state in the SIR model, the epidemic threshold has a different interpretation from that of the SIS model. Above the threshold the total number of recovered individuals reaches a finite fraction of the population, when the dynamic starts with a small fraction of infected individuals. Formally, the initial condition are: $X_{\beta\bar{\delta}}(0) = \frac{c}{n}$, $Y_{\beta\bar{\delta}}(0) = 0$ and

TABLE I: Structure and spectra of the normalized network of layers $\Phi_{\delta}^{\tilde{\gamma}}(\lambda, \eta)$. The eigenvalues assumes that the average degree of each layer, $\langle k^l \rangle$, is the same, i.e. $\langle k^l \rangle = \langle k \rangle, \forall l$.

Network	$\Phi_{\delta}^{\tilde{\gamma}}(\lambda, \eta)$	Eigenvalues
Line with 2 nodes	$\begin{bmatrix} \langle k^l \rangle & \frac{\eta}{\lambda} \\ \frac{\eta}{\lambda} & \langle k^l \rangle \end{bmatrix}$	$\begin{matrix} \langle k \rangle - \frac{\eta}{\lambda} \\ \langle k \rangle + \frac{\eta}{\lambda} \end{matrix}$
Line with 3 nodes	$\begin{bmatrix} \langle k^l \rangle & \frac{\eta}{\lambda} & 0 \\ \frac{\eta}{\lambda} & \langle k^l \rangle & \frac{\eta}{\lambda} \\ 0 & \frac{\eta}{\lambda} & \langle k^l \rangle \end{bmatrix}$	$\begin{matrix} \langle k \rangle \\ \langle k \rangle - \sqrt{2} \frac{\eta}{\lambda} \\ \langle k \rangle + \sqrt{2} \frac{\eta}{\lambda} \end{matrix}$
Multiplex	$\begin{bmatrix} \langle k^l \rangle & \frac{\eta}{\lambda} & \frac{\eta}{\lambda} \\ \frac{\eta}{\lambda} & \langle k^l \rangle & \frac{\eta}{\lambda} \\ \frac{\eta}{\lambda} & \frac{\eta}{\lambda} & \langle k^l \rangle \end{bmatrix}$	$\begin{matrix} \langle k \rangle - \frac{\eta}{\lambda} \\ \langle k \rangle - \frac{\eta}{\lambda} \\ \langle k \rangle + 2 \frac{\eta}{\lambda} \end{matrix}$

$Z_{\beta\delta}(0) = 1 - \frac{c}{n}$, where c is a small constant, $c \ll n$. Neglecting higher order terms, we have

$$\frac{dX_{\beta\delta}}{dt} = -\mu X_{\beta\delta} + \lambda \mathcal{R}_{\beta\delta}^{\alpha\tilde{\gamma}}(\lambda, \eta) X_{\alpha\tilde{\gamma}}. \quad (22)$$

After a proper factorization,

$$\frac{dX_{\beta\delta}}{dt} = \lambda \left(\mathcal{R}_{\beta\delta}^{\alpha\tilde{\gamma}}(\lambda, \eta) - \frac{\mu}{\lambda} \delta_{\beta\delta}^{\alpha\tilde{\gamma}} \right) X_{\alpha\tilde{\gamma}}, \quad (23)$$

where $\delta_{\beta\delta}^{\alpha\tilde{\gamma}}$ is a tensor analogous to the identity matrix, whose elements are one if the indices are the same. The epidemic threshold is as in eq. 20, which is the critical value for both SIR and SIS dynamics.

III. SPECTRA OF $\mathcal{R}(\lambda, \eta)$

Since the epidemic dynamics is expressed as a function of the supra adjacency tensor $\mathcal{R}(\lambda, \eta)$, studying the spectral properties of the latter could give further insights about the whole process, especially the critical point. In this section, we generalize the spectral results of interlacing, obtained in [30, 33], to the tensorial description adopted here. In addition, we also make use of the inverse participation ratio, $\text{IPR}(\Lambda)$, as a measurement of eigenvalue localization. Such ratio was firstly applied to epidemic spreading in [31], here we extend such metric to the tensorial formalism.

A. Interlacing properties

Invoking the unique mapping and considering the results of [30, 33], we can use the interlacing properties to relate the spectra of the multilayer network with the spectra of the network of layers. First of all, we define the normalized network of layers in terms of the supra contact tensor as

$$\Phi_{\delta}^{\tilde{\gamma}}(\lambda, \eta) = \frac{1}{n} \mathcal{R}_{\beta\delta}^{\alpha\tilde{\gamma}}(\lambda, \eta) U_{\alpha}^{\beta}, \quad (24)$$

where we are implicitly assuming a multilayer network in which the layers have the same number of nodes and a dependency on the spreading rates (the demonstration that such tensor is an unfolding of the matrix exposed in [30] is shown on Appendix A). Additionally, let's denote by $\mu_1 \geq \mu_2 \geq \dots \geq \mu_m$ the ordered eigenvalues of $\Phi_{\delta}^{\tilde{\gamma}}(\lambda, \eta)$. Following [30], the interlacing properties imply

$$\Lambda_{nm-m+j} \leq \mu_j \leq \Lambda_j, \quad (25)$$

for $j = m, \dots, 1$. As examples, Table I shows the spectrum of three simple networks of layers that can be computed analytically: a line with two and three nodes and a triangle. Figure 1 shows a schematic illustration of those 3 multilayer networks.

Furthermore, using similar arguments we can also obtain results for the normalized projection, formally given as

$$\mathbf{P}_{\beta}^{\alpha} = \frac{1}{m} \mathcal{R}_{\beta\delta}^{\alpha\tilde{\gamma}}(\lambda, \eta) U_{\tilde{\gamma}}^{\delta}, \quad (26)$$

whose ordered eigenvalues, denoted by $\nu_1 \geq \nu_2 \geq \dots \geq \nu_m$, also interlace with the supra contact tensor satisfying

$$\Lambda_{nm-n+j} \leq \nu_j \leq \Lambda_j, \quad (27)$$

for $j = n, \dots, 1$. Finally, the adjacency tensor of an extracted layer also interlaces, yielding to

$$\Lambda_{nm-n+j} \leq \Lambda_j^l \leq \Lambda_j, \quad (28)$$

for $j = n, \dots, 1$. These results show that the eigenvalue of the multilayer adjacency tensor is always larger than or equal to all of the eigenvalues of the individual isolated layers as well as the network of layers.

The interlacing properties presented here imply some constraints to the epidemic threshold. As advanced in [30], let $\Lambda_i(\mathcal{M})$ be the i -th eigenvalue of the tensor \mathcal{M} and consider that the set of eigenvalues is ordered as before. Moreover, for simplicity, we suppress the argument when referring to the supra-contact matrix. First of all, assuming a fixed ratio of spreading rates, we observe that the eigenvalue of the multilayer follows

$$\left(\frac{\lambda}{\mu} \right)_c^{\tilde{r}} = \frac{1}{\Lambda_1(A_{\beta}^{\alpha}(\tilde{r}))} \geq \frac{1}{\Lambda_1}, \quad \forall \tilde{r} \in 1, 2, \dots, m, \quad (29)$$

where $\left(\frac{\lambda}{\mu} \right)_c^{\tilde{r}}$ is the critical point for the single layer \tilde{r} and

$$\left(\frac{\lambda}{\mu} \right)_c^{\Phi} = \frac{1}{\Lambda_1(\Phi_{\delta}^{\tilde{\gamma}})} \geq \frac{1}{\Lambda_1}, \quad (30)$$

where $\left(\frac{\lambda}{\mu} \right)_c^{\Phi}$ denotes the critical point of the network of layers. Finally, considering the projection

$$\left(\frac{\lambda}{\mu} \right)_c^{\mathbf{P}} = \frac{1}{\Lambda_1(\mathbf{P}_{\beta}^{\alpha})} \geq \frac{1}{\Lambda_1}, \quad (31)$$

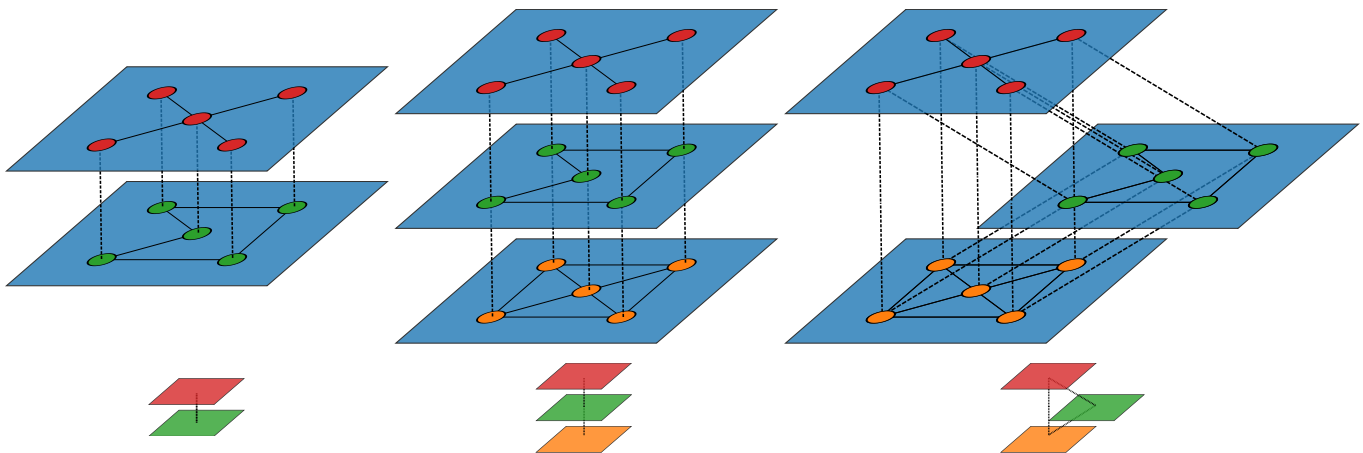


FIG. 1: (color online) Schematic Illustration of the 3 multilayer networks cases considered as examples. Top panels represent the original networks which give rise to three distinct configurations for the networks of layers. See the text for more details.

where $\left(\frac{\lambda}{\mu}\right)_c^{\mathbf{P}}$ is the critical point of the normalized projection. Thus, the spreading process on the whole system is at least as efficient as it is on the layers and on the network of layers. Note that efficiency is understood here in terms of the position of the critical point, and not regarding the fraction of infected individuals in the steady state.

B. Localization and spreading of diseases

Next, we investigate using the analysis of Section II B 2 the behavior of the system near the phase transition and whether the phenomenon of disease localization shows up. These two issues were explored for monoplex networks in [10] and [31], respectively, but have not been addressed for the case of multilayer systems. The nodal probabilities can be written as a linear combination of the eigenbasis of \mathcal{R} as

$$X_{\beta\bar{\delta}} = \sum_{\Lambda} c(\Lambda) f_{\beta\bar{\delta}}(\Lambda), \quad (32)$$

where $c(\Lambda)$ are the projections of $X_{\beta\bar{\delta}}$ on the eigentensors f . Similarly to [31], substituting such expression on the middle term of eq. 8 we obtain

$$c(\Lambda) = \sum_{\alpha\bar{\gamma}} \frac{\lambda \sum_{\Lambda'} c(\Lambda') \Lambda' f_{\alpha\bar{\gamma}}(\Lambda') f_{\alpha\bar{\gamma}}(\Lambda)}{\lambda \sum_{\Lambda'} c(\Lambda') \Lambda' f_{\alpha\bar{\gamma}}(\Lambda') + \mu}. \quad (33)$$

Considering only the contributions of the first eigenvalue and eigentensor, for $\lambda \geq \lambda_c$, the first order approximation of the macro state parameter is $\rho \approx \alpha_1 \tau$, where $\tau = \left(\frac{\lambda}{\mu} \Lambda_1 - 1\right)$, which yields

$$\alpha_1 = \frac{f_{\beta\bar{\delta}}(\Lambda_1) U^{\beta\bar{\delta}}}{nm (f_{\beta\bar{\delta}}(\Lambda_1))^3 U^{\beta\bar{\delta}}}. \quad (34)$$

Such expression is exact if there is a gap between the first two eigenvalues, as exposed in [10, 31]. Furthermore, considering two eigentensors we have $\rho \approx \alpha_1 \tau + \alpha_2 \tau^2$. Besides, following a similar approach as in [31] we can use the inverse participation ratio:

$$\text{IPR}(\Lambda) \equiv \left(f_{\beta\bar{\delta}}(\Lambda)\right)^4 U^{\beta\bar{\delta}}. \quad (35)$$

In the limit of $nm \rightarrow \infty$, if $\text{IPR}(\Lambda)$ is of order $\mathcal{O}(1)$ the eigentensor is localized and the components of $f_{\beta\bar{\delta}}(\Lambda)$ are of order $\mathcal{O}(1)$ only for a few nodes. On the other hand, if $\text{IPR}(\Lambda) \rightarrow 0$ then this state is delocalized and the components of $f_{\beta\bar{\delta}}(\Lambda) \sim \mathcal{O}\left(\frac{1}{\sqrt{nm}}\right)$.

IV. MONTE CARLO SIMULATIONS

In order to compare with analytical results, we have performed extensive numerical simulations using a Monte Carlo method from [11, 34] adapted to the case of multilayer networks, which we describe in what follows. At each time step the time is incremented by $\Delta t = \frac{1}{(\mu N_i + \lambda N_k + \eta N_m)}$, where N_i is the number of infected nodes, and N_k and N_m are the number of intra-layer and inter-layer edges emanating from them, respectively. With probability $\frac{\mu N_i}{(\mu N_i + \lambda N_k + \eta N_m)}$, one randomly chosen infected individual becomes susceptible. On the other hand, with probability $\frac{\lambda N_k}{(\mu N_i + \lambda N_k + \eta N_m)}$, one infected individual, chosen with a probability proportional to its intra-layer degree, spreads the disease to an edge chosen uniformly random. Finally, with probability $\frac{\eta N_m}{(\mu N_i + \lambda N_k + \eta N_m)}$ one infected individual, chosen with a probability proportional to its inter-layer degree, propagates the disease to an edge chosen uniformly. If an edge between two infected individuals is selected during the spreading, nothing happens, only time is incremented.

The process is iterated following this set of rules, simulating the continuous process described by the SIS scenario.

The quasi-stationary state (QS) method [11, 34] restricts the dynamics to non-absorbing states. Every time the process tries to visit an absorbing state, it is substituted by an active configuration previously visited and is stored on a list with M configurations, constantly updated. With a probability p_r a random configuration on such a list is replaced by the actual configuration. In order to extract meaningful statistics from the quasi-static distribution, denoted by $\bar{P}(n^I)$, where n^I is the number of infected individuals, the system must be on the stationary state and a large number of samples must be extracted. In this way we let the simulations run during a relaxation time t_r and extract the distribution $\bar{P}(n^I)$ during a sampling time t_a . The threshold can be estimated using the modified susceptibility [11], given by

$$\chi = \frac{\langle (n^I)^2 \rangle - \langle n^I \rangle^2}{\langle n^I \rangle} = nm \left(\frac{\langle (\rho^{QS})^2 \rangle - \langle \rho^{QS} \rangle^2}{\langle \rho^{QS} \rangle} \right), \quad (36)$$

where ρ^{QS} is the quasi-stationary distribution $\bar{P}(n^I)$. As argued in [11, 34] the susceptibility presents a peak at the phase transition on finite systems. Such measure is the coefficient of variation of the temporal distribution of states over time on the steady state. Note that the magnitude of the susceptibility χ is not of primary interest to us, but rather the position of its maximum value with respect to μ/λ , since it will coincide with the critical threshold for sufficiently large systems.

In addition, after obtaining the curves of $\chi \times \lambda$ by the QS method, we also apply a moving average filter in order to get rid of the noise. Such an approach improves the visual quality of the plots and does not interfere on the results, since the epidemic spreading presents only second order (i.e. continuous) phase transitions, and the order of magnitude of the noise is smaller than those of the peaks corresponding to the phase transitions.

The parameters used in the QS method are $p_r = 0.01$, $t_a = 10^6$ and t_r varies from 10^6 to 3×10^6 in order to obtain a smoother curve. The QS method demands a large sample size, since it is estimating the variance of a distribution. Moreover, we construct the $\chi \times \lambda$ curves in steps of $\Delta\lambda = 10^{-3}$ and the moving average window has 5 points.

V. 2-LAYER MULTIPLEX SYSTEMS

In this section we numerically study 2-layer multiplex systems. First, we focus on the phase diagram of the spreading process as a function of the inter and intra layer spreading rates for both, SIS and SIR scenarios. Next, we analyze the spectral properties of such systems, comparing with results of Section III. Finally, we perform Monte Carlo simulations that show the existence of multiple phase transitions on multiplex networks. The latter

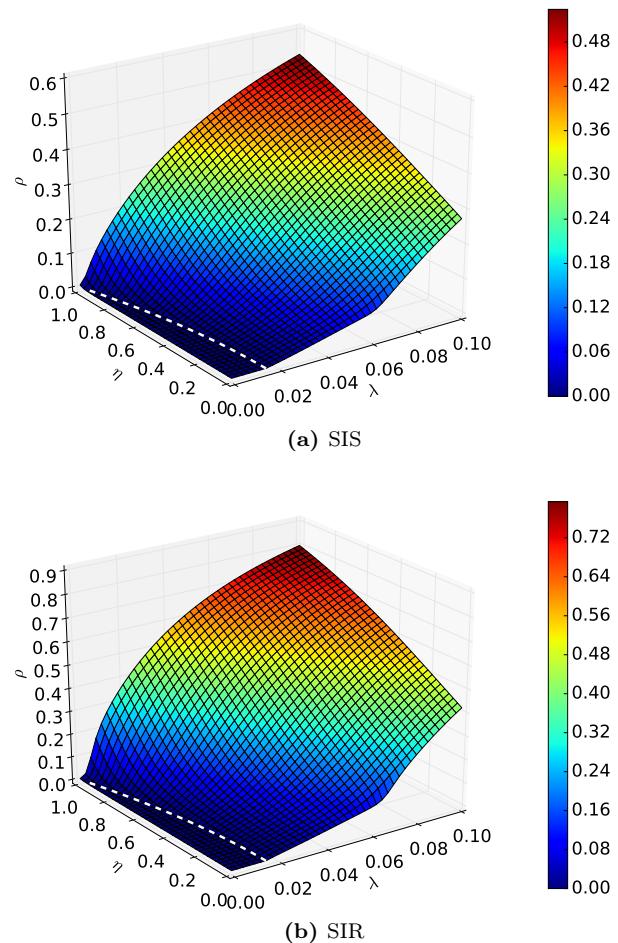


FIG. 2: Phase diagrams over a 2-Layer multiplex system, where each layer has $n = 10^4$ for a fixed value of $\mu = 1$. (a) Density of spreaders as a function of the parameters η and λ . (b) Density of recovered individuals as a function of the parameters η and λ . Colors represent the fraction of spreaders and the white line is the threshold calculated using equation 20.

results are analyzed in terms of the spectral properties of $\mathcal{R}(\lambda, \eta)$.

A. Numerical solution

Results shown in this section are the numerical solutions of the ODE systems 5 and 21 using a Runge-Kutta (4,5) algorithm [35]. We consider a 2 layer multiplex network ($m = 2$), where each layer has $n = 10^4$ nodes. In order to build a multiplex network where the epidemic thresholds associated to the individual layers are well separated, we must guarantee that $\Lambda_1^l \gg \Lambda_2^l$. Therefore, we chose the degree distribution of the first layer to be $P(k) \sim k^{-2.5}$, whereas that of the second layer is $P(k) \sim k^{-4.5}$. Both layers are created using the uncorre-

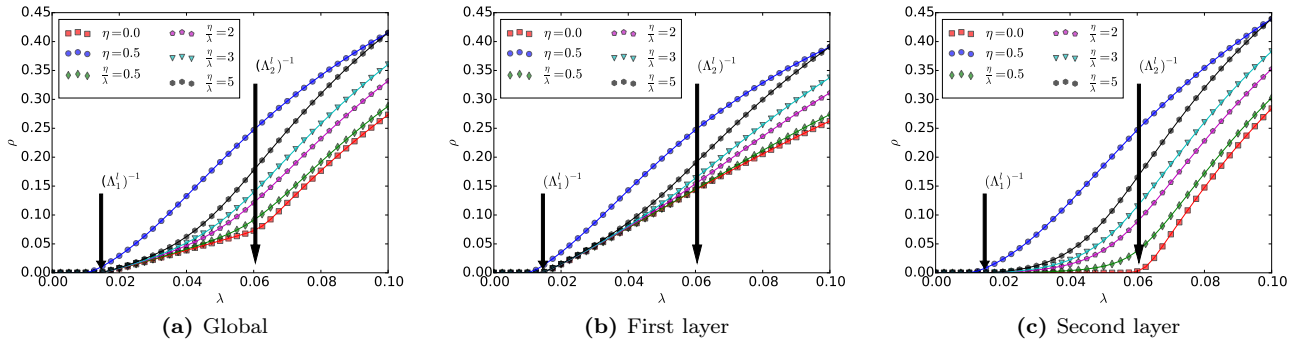


FIG. 3: Individual layer behavior over a 2-Layer multiplex system. Each layer has $n = 10^4$ for a fixed value of $\mu = 1$. The results considering both layers are shown in (a), while the dynamics in the individual layers are shown in (b) ($P(k) \sim k^{-2.5}$) and (c) ($P(k) \sim k^{-4.5}$). The arrows indicate the layers leading eigenvalues.

lated configuration model [36]. Moreover, we consider a multilayer network in which every node has its counterpart on the other layer. This pairing of nodes of different layers is made randomly. Each result is the solution considering one single (and fixed) multiplex network.

Figure 2 shows the phase diagram considering the average fraction of spreaders for the SIS dynamics (or recovered for the SIR dynamics) as a function of the spreading parameters λ and η for a given recovering rate $\mu = 1$. The dashed white line denotes the epidemic threshold obtained from eq. 20. In (a) we show the SIS scenario, while in (b) corresponds to the SIR model. In both cases, it is possible to observe two changes on the system's behavior. The first on the epidemic threshold, while the second near the epidemic threshold of the second layer. In addition, we note the agreement between the theoretical epidemic thresholds and the numerical results. Furthermore, the higher the η , the lower the epidemic threshold tends to be, which is a consequence of the eigentensor problem. Also note that ρ increases, for a fixed λ as η increases, even for $\lambda \sim 0$, which means that in such extreme cases, the disease spreads mainly on the interlayer edges.

Figure 3 shows the phase diagram for $\mu = 1$ and different values of the parameter η for the SIS dynamics. For $\eta = 0$ we have no inter-layer spreading, while for $\eta = 0.5$ we have a fixed spreading rate, independent of the intra-layer rates. In addition, we also evaluated cases where the ratio $\frac{\eta}{\lambda}$ is constant. In Fig. 3 (a) we have the global behavior of the system, which is an average of the individual behavior of the layers, represented in panels (b) and (c), since both layers have the same number of nodes. Furthermore, we also observe that the two individual networks show different behaviors near the epidemic threshold [10]. The first layer (Fig. 3 (b)) has a lower epidemic threshold than the second. However ρ grows (as a function of λ) slower than in the second. This feature can be observed clearly in Fig. 3 (b) and (c), where we show results for $\eta = 0$, that is, when there is no spreading

between the layers.

Considering the discrete system [28], Cozzo et al. verified the shifting on the dominated layer (the largest amongst all individual eigenvalues) as the ratio $\frac{\eta}{\lambda}$ increases. Here we observe the same effect, as can be seen in Fig. 3 (c). Additionally, we can also note another global change approximately beyond $\lambda > (\Lambda_2^l)^{-1}$. Our findings suggest the possibility of multiple phase transitions due to the multiplex structure of the network. It is noteworthy that in spite of the similarities between our continuous model and the discrete model [28], both represent slightly different processes. On the continuous case, two events cannot happen at the same time. On the other hand, on the discrete model, every node contacts its neighbors on one discrete time step. Despite these differences, the results show that both the continuous and discrete formulations are phenomenologically similar.

B. Spectral analysis

In this section we focus on the spectral analysis of the tensor $\mathcal{R}(\lambda, \eta)$ as a function of the ratio $\frac{\eta}{\lambda}$. Here we focus on three special cases in increasing order of complexity: (i) the identical case, where both layers are exactly the same. Thus, there is a high correlation between the degree on each layer; (ii) the non-identical case, where both layers present the same degree distribution, but different configurations and (iii) different layer structures, so that their corresponding eigenvalues are spaced.

1. Identical layers

We consider a multiplex network made up of two layers with the same configuration. Each layer of the multiplex is a network composed by $n = 1000$, $\langle k \rangle \approx 6$, $\Lambda^l = 14.34$, with degree distribution $P(k) \sim k^{-2.7}$. Aside from the intra-edge configuration, we also impose that inter-edges

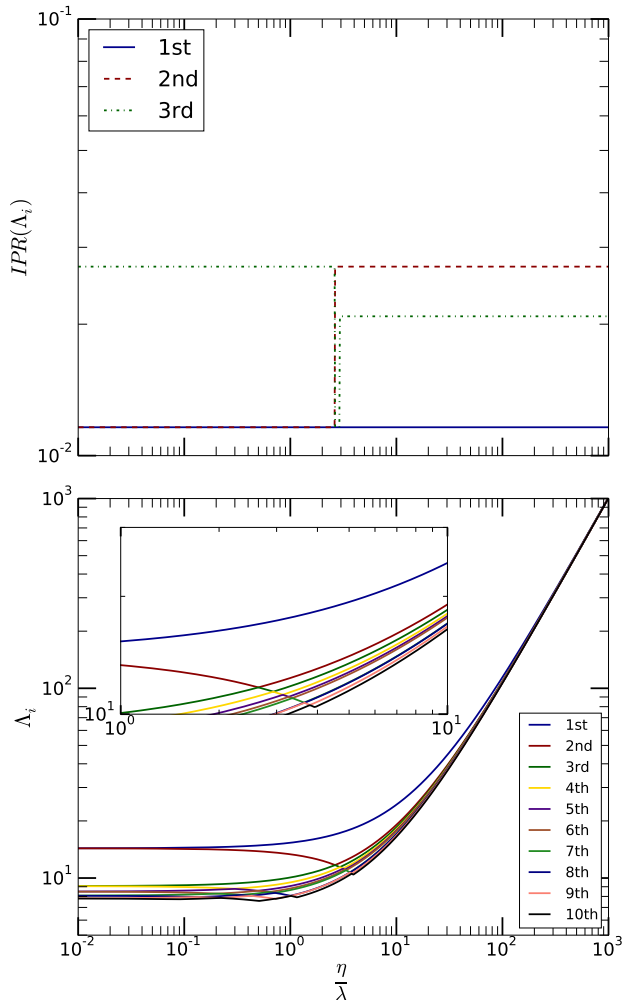


FIG. 4: Spectral properties of the tensor $\mathcal{R}(\lambda, \eta)$ as a function of the ratio $\frac{\eta}{\lambda}$ for a multiplex with two layers with the exact same degree distribution and connected to its counterpart on the other layer. On the top panel we present the inverse participation ratio ($\text{IPR}(\Lambda)$) of the three larger eigenvalues, while on bottom panel we show the leading eigenvalues. Every curve is composed by 10^3 log spaced points, in order to have enough resolution.

connect a node with its counterpart on the other layer, i.e., every node has the same intra-degree on all layers. Such a constraint imposes a high correlation between the degrees on each layer.

Figure 4 shows the spectral behavior of such a multiplex as a function of the parameter $(\frac{\eta}{\lambda})$. On the top panel, we represent the inverse participation ratio of the first three eigenvalues, while on the bottom panel, we plot the first ten eigenvalues. When the ratio $\frac{\eta}{\lambda} = 0$ the eigenvalues have multiplicity two, as can be seen on the left side of the bottom panel (approximately, since the figure starts from 10^{-2}). More importantly, those eigenvalues tend to behave differently: one increases, while

the other tends to decrease. This behavior leads to the eigenvalue crossing (see Appendix B). The inset of the bottom panel zooms out the region where the crossing takes place. Note that the eigenvalues cross at the same value for which the inverse participation ratio shows an abrupt change. Indeed, the jump in the $\text{IPR}(\Lambda)$ has its roots in the interchange of the eigenvectors associated to each of the eigenvalues that are crossing. Moreover, we stress that the abrupt change observed for $\text{IPR}(\Lambda)$ is always present in such scenarios, but it could be either from the lower to the higher values or vice versa depending on the structure of the layers.

2. Similar layers

In addition to the identical case, we have also considered a multiplex network composed by two layers with the same degree distribution (i.e. the same degree sequence), with $P(k) \sim k^{-2.7}$, but different random realizations of the configuration model. Furthermore, the inter-edges follow the same rule as before, connecting nodes with their counterparts on the other layer assuring that every node has the same intra-degree on all layers. Each layer of the multiplex network is composed by $n = 1000$ and $\langle k \rangle \approx 6$. Since each layer is a different realization of the configuration model, both present a slightly different leading eigenvalue, the first $\Lambda_1^1 = 15.21$ and the second $\Lambda_1^2 = 14.34$.

Figure 5 shows the spectral behavior of such a multiplex in terms of the largest eigenvalues, on the bottom panel, and the $\text{IPR}(\Lambda)$, on the top panel. Here, in addition to the global inverse participation ratio, we also present the contribution of each layer to this measure. Such analysis is meaningless on the identical case, since the contribution is the same. As shown in the figure, we observe that for small values of $\frac{\eta}{\lambda}$, in regard to the first eigenvalue, the system is localized on the first layer and delocalized on the second. On the other hand, the picture changes when we focus on the second eigenvalue, as it is localized on the second layer, but delocalized on the first. For larger values of $\frac{\eta}{\lambda}$, both layers contribute equally to $\text{IPR}(\Lambda)$. Analogously to the identical case, there is a change on $\text{IPR}(\Lambda_2)$, which seems to be related to the changes on Λ_2 , as one can see on the bottom panel and in the inset. Note that for this case, there is no crossing, i.e., the eigenvalues avoid the crossing -also referred to as near-crossing.

3. Different layers

Although the two cases evaluated previously present interesting spectral behaviors, both represent scenarios in which the eigenvalues of each layer are similar, if not the same. Next, we study a multiplex network made up of two scale-free networks with $\gamma \approx 2.2$ and $\gamma \approx 2.8$. Such a configuration imposes a distance between the leading

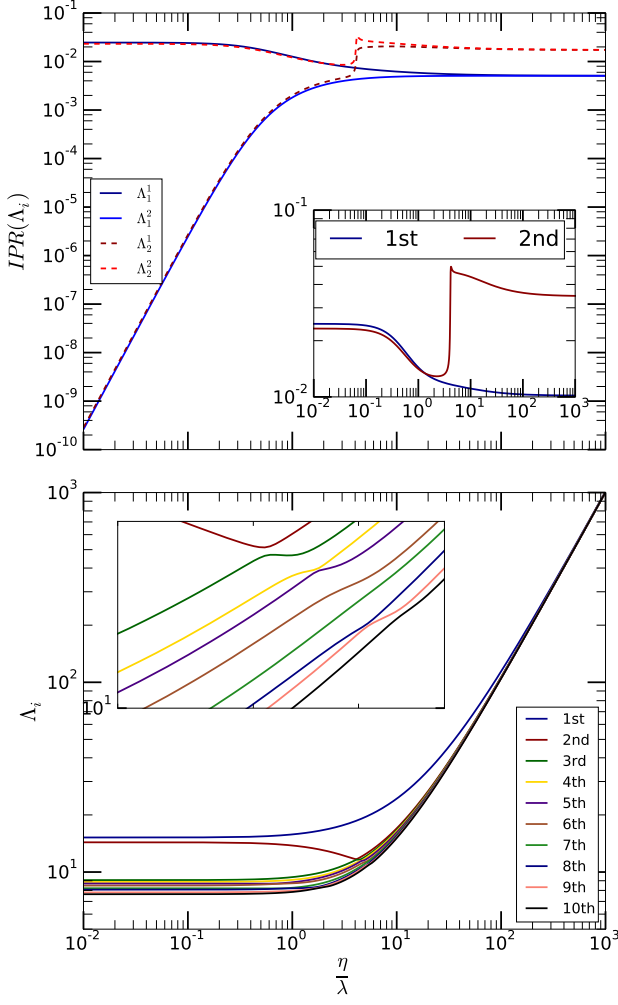


FIG. 5: Spectral properties of the tensor $\mathcal{R}(\lambda, \eta)$ as a function of the ratio $\frac{\eta}{\lambda}$ for a multiplex with two layers with the same degree distribution (different random realizations of the configuration model) and connected to its counterpart on the other layer. On the top panel we present the inverse participation ratio ($IPR(\Lambda)$) of the two larger eigenvalues and the individual layer contributions, while on bottom panel we show the leading eigenvalues. Every curve is composed by 10^3 log spaced points, in order to have enough resolution.

eigenvalues of each layer, and therefore we expect a completely different behavior with respect to the previous setups. Both layers have $\langle k \rangle \approx 8$ and $n = 10^3$ nodes on each layer and the leading eigenvalues are $\Lambda_1^1 = 42.64$ for the first and $\Lambda_1^2 = 21.29$ for the second.

Figure 6 shows the spectral properties of the tensor $\mathcal{R}(\lambda, \eta)$ as a function of the ratio $\frac{\eta}{\lambda}$. In contrast to the identical and similar cases, figures 4 and 5, where some eigenvalues increase while others decrease, here all the observed eigenvalues always increase. Moreover, we do not observe any crossing or near-crossing behavior. Regarding $IPR(\Lambda)$, the same pattern as for the similar case

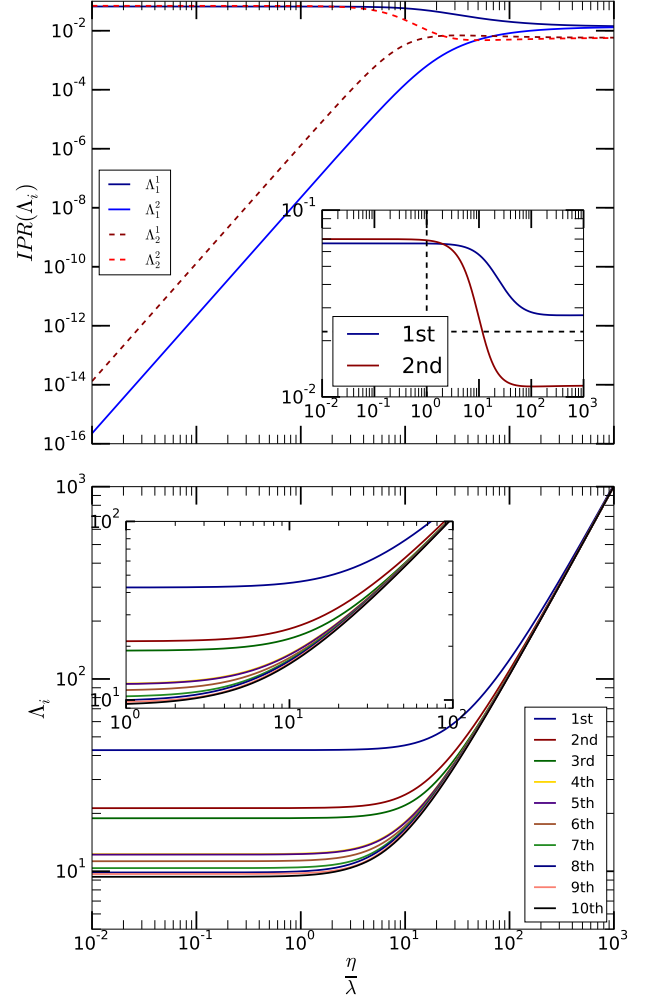


FIG. 6: Spectral properties of the tensor $\mathcal{R}(\lambda, \eta)$ as a function of the ratio $\frac{\eta}{\lambda}$ for a multiplex with two layers, the first with $\gamma \approx 2.2$, while the second $\gamma \approx 2.8$. Both have $\langle k \rangle \approx 8$. On the top panel we present the inverse participation ratio ($IPR(\Lambda)$) of the two larger eigenvalues and the individual layer contributions, while on bottom panel we show the leading eigenvalues. Every curve is composed by 10^3 log spaced points, in order to have enough resolution.

is found: for small values of $\frac{\eta}{\lambda}$ and considering the first eigenvalue, the system appears localized on the first layer and delocalized on the second, while for $IPR(\Lambda_2)$, it is the contrary. For larger values of $\frac{\eta}{\lambda}$, both layers contribute equally to the $IPR(\Lambda)$. The only difference that we observe for the current setup with respect to the two similar networks (see Figure 5), is that now no drastic change on the inverse participation ratio is found, as expected, since there is no near-crossing.

From figure 6 we can also extract an important numerical result regarding the perturbation theory. We observed that in our case, considering a two spaced-individual layer eigenvalues problem, the leading eigen-

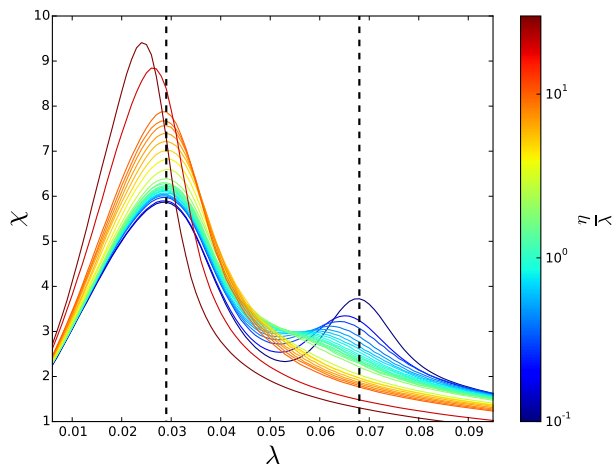


FIG. 7: Susceptibility, χ , as a function of the spreading rate λ for different ratios of inter and intra-layer spreading ratings, $\frac{\eta}{\lambda}$ for a fixed value of $\mu = 1$ over a 2-Layer multiplex system, where each layer have $n = 10^3$, the first with $\gamma \approx 2.2$, while the second $\gamma \approx 2.8$. Both have $\langle k \rangle \approx 8$. The simulated values are $\frac{\eta}{\lambda} = 0.1, 0.2, 0.3, 0.4, 0.5, 0.6, 0.7, 0.8, 0.9, 1.0, 1.1, 1.2, 1.3, 1.4, 1.5, 1.6, 2, 3, 4, 5, 6, 7, 8, 9, 10, 20, 30$.

value can be approximated by the largest leading eigenvalue of the individual layers for $\frac{\eta}{\lambda} \lesssim 1$, such approximation becomes poorer as $\frac{\eta}{\lambda}$ increases, but it can be acceptable up to $\frac{\eta}{\lambda} \lesssim 10$, within a certain error. Apart from that, note that both eigenvalues tend to increase, while its difference tends to decrease.

C. Multiple phase transitions

In [34] Mata and Ferreira showed that it is possible to have multiple transitions on monoplex networks. They studied the behavior of a SIS model on networks with $\gamma > 3$. Here we show that such phenomena also appear, in a natural way, on multilayer networks. Motivated by the findings reported in the latter sections, especially by the presence of a second transition as observed in Figures 2 and 3, we have performed extensive Monte Carlo simulations using the QS-method with the aim of determining as accurately as possible the points at which the phase transition takes place for a 2-layer multiplex network. Here we use the mutiplex built up in Section V B 3, since the leading eigenvalues of each layer are spaced. Note that our numerical simulations are performed on a fixed network, since we follow the quenched formalism.

Figure 7 shows that for low values of the ratio $\frac{\eta}{\lambda}$, both networks are weakly coupled and the system exhibits two well-defined critical points (vertical dotted lines). However, as this ratio increases the peak signaling the presence of the second critical point decreases and eventually vanishes. In our simulations, we have observed that up to $\frac{\eta}{\lambda} \approx 1$, the second peak, although less defined, is still

present. Beyond the latter point, only one peak remains. As $\frac{\eta}{\lambda}$ further increases, the position of the remaining critical point remains the same, and the peak is even more well defined. Interestingly enough, if the ratio $\frac{\eta}{\lambda}$ continues to increase -in our numerics beyond $\frac{\eta}{\lambda} \gtrsim 10$ - the critical point shift to the left to values that are even smaller than the smallest critical point of the individual layers. It is worth highlighting that a similar qualitative behavior can be seen in the results shown in Fig. 2 (a), where one can also observe a second phase transition -note the change in the slope of ρ near the leading eigenvalue of the second layer. This transition also vanishes as the intra-layer spreading increases.

Since the tensor $\mathcal{R}(\lambda, \eta)$ plays a major role on the spreading process, our spectral results can help understand the observed critical dynamics. In epidemiological terms -or in general for contagion processes-, the localization of the disease on a certain layer means that most of the spreading is expected to take place on the nodes of that layer. Moreover, in addition to the localization on the layers, one can also have localization effects on specific nodes or groups of nodes for instance.

In order to analytically explain this phenomenon, we evaluate $\text{IPR}(\Lambda)$ for the two leading eigenvalues, as this measure indicates the localization of an eigenstate, see Section V B 3 (results shown in Figure 6). Comparing the susceptibility and $\text{IPR}(\Lambda)$, we observe that $\text{IPR}(\Lambda_2)$ starts decaying for $\frac{\eta}{\lambda} \approx 1$ and crosses the value $\frac{1}{\sqrt{nm}}$, at which the associated eigenvector delocalizes, for $\frac{\eta}{\lambda} \approx 10$, that compares well with the point at which the second peak in the susceptibility decays and finally disappears. Moreover, $\text{IPR}(\Lambda_1)$ decays from $3 \lesssim \frac{\eta}{\lambda} \lesssim 10$, which coincides with the range where the remaining maximum in the susceptibility reaches higher values and is better defined. More interestingly, note that $\text{IPR}(\Lambda_1)$ is mainly composed by the contributions of the first layer for a lower spreading ratio, suggesting that it is localized on such layer. Therefore, our results suggest that the $\text{IPR}(\Lambda)$ is a proper measure to detect and predict the observed two phase transitions in the system's behavior and potentially for m -phase transitions, as we will show in the next section.

VI. 3-LAYER INTERCONNECTED SYSTEMS

Following the main ideas of the last sections, we next explore what happens for multilayers networks with are made by more of two layers. Specifically, we have carried out numerical simulations for a 3-layer system. We generate multiplex networks using three scale-free networks, with $\gamma \approx 2.3$, $\gamma \approx 2.6$ and $\gamma \approx 2.9$, with $\langle k \rangle \approx 8$ and $n = 10^3$ nodes on each layer. Note that we consider three layers with spaced individual leading eigenvalues in order to investigate whether multiple phase transitions is a generic phenomenon of multilayer systems. Note that we have two possible topologies for the network of layers: (i) a line graph and (ii) a triangle (which is a node-

aligned multiplex). In its turn, the first can be arranged in three possible configurations by changing the central layer. That is, we have four possible systems. We perform our numerical simulations as in the last Section.

First, we evaluate the spectrum of $\mathcal{R}(\lambda, \eta)$ for all the networks described. In the following, we apply the localization theory in order to get insights on the dynamical behavior, similarly to Section V C.

A. Spectral analysis

Since the epidemic process is described through the supra adjacency tensor $\mathcal{R}(\lambda, \eta)$, its spectral properties give us some insights about the whole process, especially about the critical properties of the systems under analysis. Moreover, as the structure of the network of layers is not trivial anymore, we shall find important differences regarding the spectra of such tensors for the different topologies of the network of layers.

1. Spectrum

Figure 8 shows the spectrum of the four configurations of networks when varying the ratio $\frac{\eta}{\lambda} = 1, 10, 100$ and 1000. Observe that we do not show the ratio $\frac{\eta}{\lambda} = 0$ since it is just the union of the individual layers' spectrum. For $\frac{\eta}{\lambda} = 1$, the four configurations are very similar, especially the line graphs. In such case, the inter-layer edges are treated in the same way as the intra-layer ones. In other words, they are ignored and the network can be interpreted as a monoplex network. As the spreading ratio increases the spectrum tends to be clustered near the values of the eigenvalues of the network of layers. Such spectra was analytically calculated in Section II and shown in Table I.

Regarding the triangle configuration, the clustering of the spectrum as $\frac{\eta}{\lambda}$ increases is even clear. Triangles present the lowest eigenvalue with multiplicity two. On the extreme case of $\frac{\eta}{\lambda} \gg 1$, see Figure 8, we have 2/3 of the values near the left extreme value while 1/3 is near the leading eigenvalue. On the other hand, for the line configurations, the frequencies of the eigenvalues distribution is related to the position of the central layer. However, on the limiting cases such differences are reduced. This pattern is naturally related to the increase of the spreading ratio: When $\frac{\eta}{\lambda}$ increases, so does the role of the inter-layer edges relative to the intra-layer ones. Consequently, the structure of the network of layers imposes itself more strongly on the eigenvalues of the entire interconnected structure. This comes as a consequence of the interlacing theorems shown in Section II B 2.

Our findings can be related to the structural transition shown in [37], where the authors evaluated the supra-Laplacian matrix as a function of the inter-layer weights. Their main result is an abrupt structural transition from a decoupled regime, where the layers seem

to be independent, to a coupled regime where the layers behave as one single system. Here, we are interested in the supra-adjacency tensor, however, we found a similar phenomenological behavior and a structural change of the system as a function of the inter-layer weights, which in our case are determined by a dynamical process.

2. Localization on interconnected networks

Apart from the eigenvalues distribution, it is also important to analyze the eigentensors. Such an analysis is performed in terms of the inverse participation ratio, similarly to what we did for the 2-Layer multiplex case.

Figure 9 shows the 10th larger eigenvalues of the 3-layer multiplex case. The dashed lines represent the leading eigenvalue of each layer. Note that the leading eigenvalue of the layer with $P(k) \sim k^{-2.9}$ is the 7th larger on the network spectrum when $\frac{\eta}{\lambda} = 0$. We observe that there is no crossings on the observed eigenvalues, which is an expected result, since the layers have different structures. Furthermore, it is important to remark that all networks of layers evaluated also show similar qualitative behaviors. The topology of the network of layers does not lead to qualitative differences on the dependence of Λ_i on $\frac{\eta}{\lambda}$ for the first ten eigenvalues. We also notice that although it is only an approximation, the perturbation theory would be valid roughly up to $\frac{\eta}{\lambda} \lesssim 10$.

Figure 10 shows the $\text{IPR}(\Lambda_1)$. On the main panel we present the individual contribution of each layer, while on the insets we have the total $\text{IPR}(\Lambda_1)$. An interesting phenomenon can be observed comparing the different line configurations of the network of layers. The largest eigenvalue of the whole system, Λ_1 , has its associated eigenvector localized in the dominant layer, that is, in the layer generated using $\gamma = 2.3$. Depending on the position of that layer in the whole system — i.e., central or peripheral layer —, the contribution of the non-dominant layers to $\text{IPR}(\Lambda_1)$ varies. In particular, when the dominant layer corresponds to an extreme node of the network of layers, the contribution of the other two layers will be ordered according to the distance to the dominant one. Consequently, when the dominant layer is in the center of the network of layers, the contributions of the non-dominant ones are comparable -note that in panel c) of Figure 10, there is no difference in the contribution to $\text{IPR}(\Lambda_1)$ of layers generated using $\gamma = 2.6$ and $\gamma = 2.9$.

As for the first eigenvalue, which is usually enough to analyze the localization as a first order approximation, we observe that the layer with the largest eigenvalue dominates the dynamics. In addition, note the similarities between the multiplex and the line configuration ($2.6 + 2.3 + 2.6$), where the non-dominant layers behave similarly. This is because for small values of $\frac{\eta}{\lambda}$, the effect of the extra edge in the network of layers (closing the triangle) is of order η^2 and so the similar behavior observed in panel c) and d) of Figure 10 for the two configurations. As $\frac{\eta}{\lambda}$ grows, the symmetry in the node-aligned multiplex

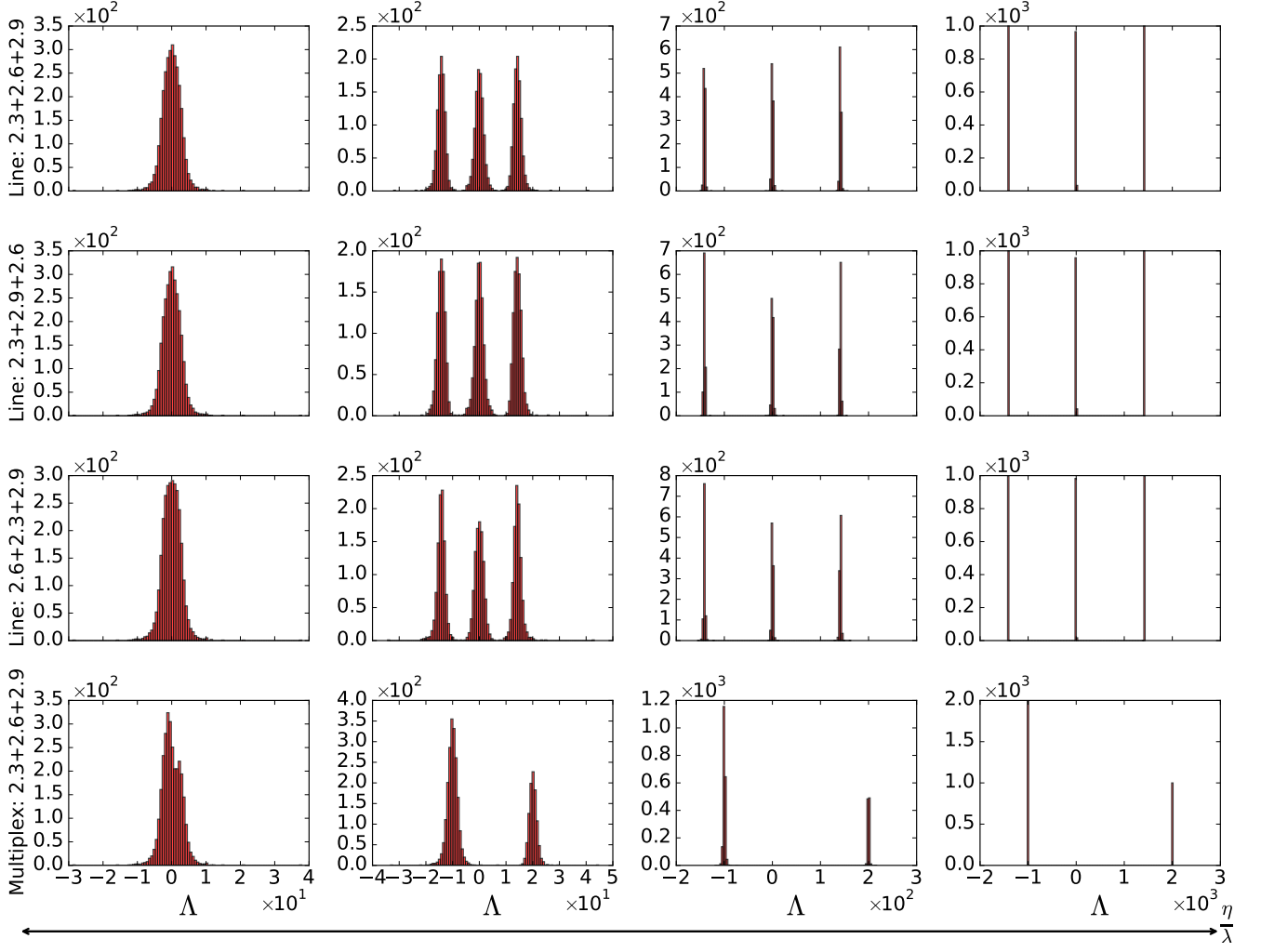


FIG. 8: Distribution of the eigenvalues. On the rows, from top to bottom, for the interconnected networks of Lines 2.3+2.6+2.9, 2.3 + 2.9 + 2.6, 2.6 + 2.3 + 2.9 and the multiplex. On the columns, from left to right, we varied the ratios $\frac{\eta}{\lambda} = 1, 10, 100$ and 1000 respectively. All histograms were built with 100 bins.

dominates the eigenvector structure and the contributions of all layers are comparable. As we next show, the different contributions of the layers to the total $\text{IPR}(\Lambda_1)$ are at the root of the multiple transitions observed.

B. Multiple phase transitions

Figure 11 shows the susceptibility as a function of λ for different ratios of $\frac{\eta}{\lambda}$. We observe three well defined peaks on such curves when the ratio $\frac{\eta}{\lambda}$ is small. In addition, similar to the 2-layer case, such peaks tend to become less defined and vanish as the ratio $\frac{\eta}{\lambda}$ increases. The third peak is less defined than the others because the average number of infected nodes is larger in this case. Consequently the susceptibility tend to be lower, since it measures the variance in relation to the average. Such observation suggests that it could be harder to observe

peaks for non-dominating layers that have an individual critical point too far from the dominating layer.

Except for the line (2.3 + 2.9 + 2.6) all figures are similar and present similar peaks, implying that the phase transitions occur approximately at the same point. On the other hand, the line (2.3 + 2.9 + 2.6) shows a slightly different behavior for the second peak, that is found for a larger value of λ than for the other cases. Such result suggests that when the layer with the largest eigenvalue is located at the center of the line, it can effectively act as a barrier to the disease. In addition, it is verified that the extra inter-edges of the multiplex case does not lead to radical changes on the transition points. We remark that the susceptibility does not measure the fraction of spreaders in the steady state, thus, despite of the similarities of those curves, the phase diagrams for the incidence of the disease are different.

Coming back to what is observed for the network of

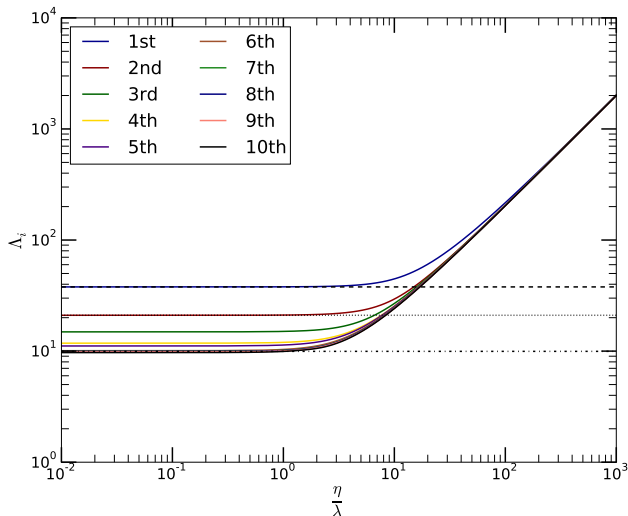


FIG. 9: Evaluation of the 8 first eigenvalues of $\mathcal{R}(\lambda, \eta)$ for the multiplex configuration as a function of the ratio $\frac{\eta}{\lambda}$. It is noteworthy that such plot is visually equivalent for all the layer topologies composed by 3 layers. The dashed lines represents the individual layer leading eigenvalues.

layers described by the line $(2.3 + 2.9 + 2.6)$, an interesting phenomenon arises, namely, the formation of barriers to the epidemic spreading. Since the middle layer has the lowest individual eigenvalue among the layers, it creates a barrier effect “delaying” the second transition. Moreover, we observe that such transition also vanishes for higher values of the ratio $\frac{\eta}{\lambda}$, if compared to the other cases. This can be related to the inverse participation ratio of Λ_1 , $\text{IPR}(\Lambda_1)$, shown in Figure 10. Note that, for the line $(2.3 + 2.9 + 2.6)$, the contribution of the layer $\gamma = 2.6$ is the lowest. As shown in Section V A (and in [28]), for a 2-layer multiplex, the non-dominant layer has its critical point shifted to a lower value of the spreading rate, which means that the outbreak takes place before it would have happened if that layer were isolated. However, here such shifting is compromised by the fact that the central layer is unable to sustain the epidemic process, acting effectively as a barrier for disease contagion. Apart from this new effect, the system behaves qualitatively similar to the 2-layer scenario.

VII. CONCLUSIONS

In this paper, we have generalized and extended previous analysis to the case of multilayer networks. To this end, we have made use of the tensorial representation introduced in [29], which allows to extract upper and lower bounds for the disease incidence of a SIS model and the critical points for both, the SIS and the SIR dynamical processes. We have also validated our analytical insights with extensive numerical simulations, recovering results

like those presented in [28] regarding the shifting of the global epidemic threshold to lower values of the spreading rate and the role of the so-called dominant layer. Furthermore, we have observed a transition on the spectra of the supra-contact tensor, from the spectra resulting from the union of the individual layers to the spectra of the network of layers. Such a behavior suggests that other dynamics and more complex structures can also be significantly affected by the interconnected nature of the system. In addition, we also have characterized analytically the phenomenon of eigenvalue crossing on the supra-contact tensor for two identical layers case. It is worth noticing that any dynamical process that is described by the same matrix will be affected by this effect.

Our main results concern the emergence and vanishing of multiple transitions as a function of the ratio between the inter-layer and intra-layer spreading rates and their relation to the spectral properties of the multilayer, which also reveal the phenomenon of disease localization, in particular, its relation with the existence of crossings or near-crossings of eigenvalues. Using the QS-Method and Monte Carlo simulations, we have been able to precisely determine the transition points. Our results show that it is possible to have multiple phase transitions in multilayer networks, as previously claimed for monoplex systems [34]. Additionally, we have proposed an analytical approach based on the use of the inverse participation ratio to characterize such transitions as a localization phenomenon, thus also connecting with [31]. A detailed exploration of the parameter space show that as the ratio between the inter-layer and intra-layer spreading rates increases, the peaks of the susceptibility measured for the non-dominant layers tend to occur at lower values of λ and vanish as $\frac{\eta}{\lambda}$ increases up to a point in which only one phase transition is observed. Interesting enough, our results point out that such a transition can take place for even lower values of λ than the inverse of the largest leading eigenvalue among all individual layers. Finally, another important finding presented here is the opposite effect, namely, the fact that a phase transition can take place for a larger value of λ than expected as a consequence of the multiplex topology. Specifically, if the layers are arranged in such a way that one with the smallest leading eigenvalue is at the center of the network of layers (for instance, as happens for the line $(2.3 + 2.9 + 2.6)$ configuration), then the corresponding transition could be delayed due to a barrier effect. Summarizing, our results emphasize the importance of studying multilayer systems as they are and not only their individual layers.

Acknowledgments

FAR acknowledge CNPq (grant 305940/2010-4), Fapesp (2013/26416-9). GFA acknowledges Fapesp for the sponsorship provided (grants 2012/25219-2 and 2015/07463-1). E. C was supported by the FPI program of the Government of Aragón, Spain. This work has been

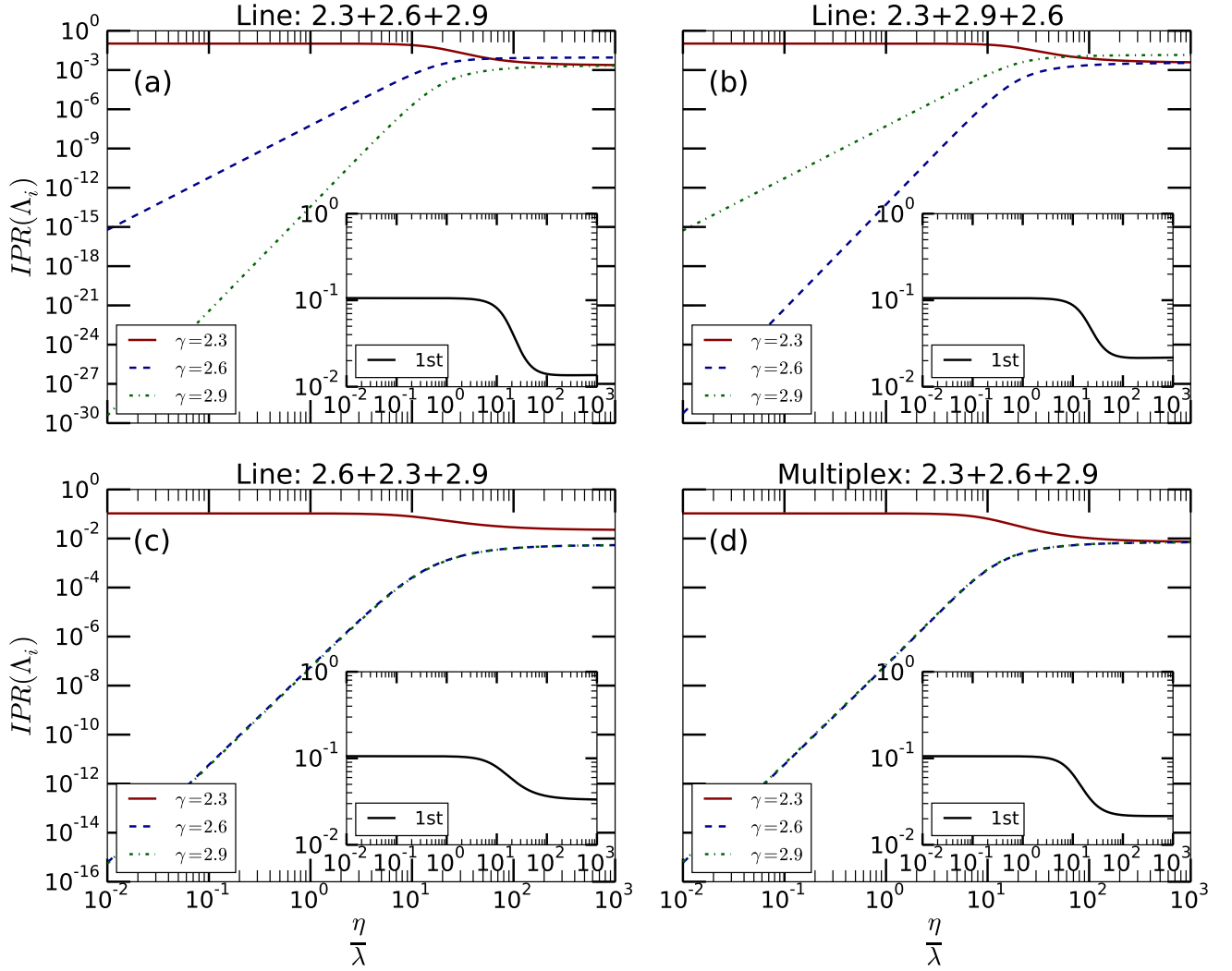


FIG. 10: Contribution of each layer to the inverse participation ratio for the first eigenvalue of $\mathcal{R}(\lambda, \eta)$ considering all three layer configurations as a function of the ratio $\frac{\eta}{\lambda}$. On the inset we show the behavior of $IPR(\Lambda_1)$. Such eigenvalue is related to the leading eigenvalue of the layer $\gamma = 2.3$ when $\frac{\eta}{\lambda} = 0$.

partially supported by a grant to the group FENOL and by the EC FET-Proactive Project PLEXMATH (grant 317614).

Appendix A: Proof of Equation 24

Considering the matricial representation of a multi-layer network, given by

$$A = \oplus_{\alpha} A^{\alpha} + C = \begin{bmatrix} A_1 & C_{12} & \cdots & C_{1m} \\ C_{21} & A_2 & \cdots & C_{2m} \\ \vdots & \vdots & \ddots & \vdots \\ C_{m1} & C_{m2} & \cdots & A_m \end{bmatrix} \quad (37)$$

where $A \in \mathbb{R}^{nm \times nm}$, $A^{\alpha} \in \mathbb{R}^{n \times n}$ is the adjacency matrix of the layer $\alpha \in \{1, 2, \dots, m\}$ and C is a coupling matrix. Since we assume multilayer network in which the layers have the same number of nodes we have $C_{ij} = I$. Assuming a partition of such network, represented by $S \in \mathbb{R}^{nm \times m}$, which is the characteristic matrix of such partition, where $S_{ij} = 1$ if $i \in V_j$ and zero otherwise, where V_j is the network of layers partition.

In order to use the results of [30, 33] we have to prove that our tensor $\Phi_{\delta}^{\tilde{\gamma}}(\lambda, \eta)$ is an unfolding of the network of layers matrix \bar{R} [30, 33], formally given by

$$\bar{R} = \Gamma^{-1} S^T A S, \quad (38)$$

where Γ is a diagonal matrix with normalizing constants (for more, see references [30, 33]). In words, the prod-

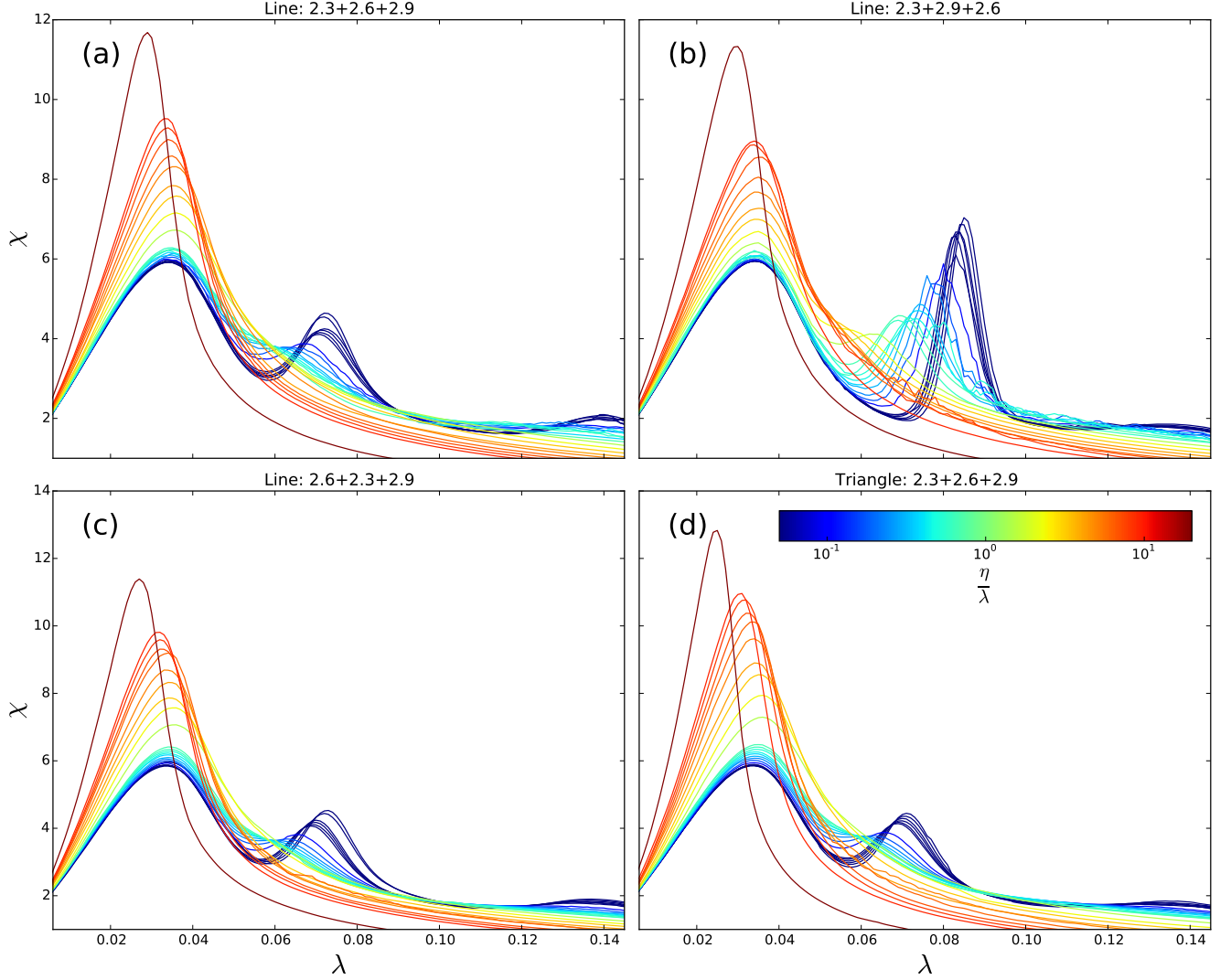


FIG. 11: Susceptibility χ as a function of λ considering all three layer configurations and many different ratios $\frac{\eta}{\lambda}$, which is represented by the color of the lines. The recovering rate is $\mu = 1$. The simulated values are $\frac{\eta}{\lambda} = 0.05, 0.06, 0.07, 0.08, 0.09, 0.1, 0.2, 0.3, 0.4, 0.5, 0.6, 0.7, 0.8, 0.9, 1.0, 2, 3, 4, 5, 6, 7, 8, 9, 10, 20$.

uct AS is a summation over the blocks of the matrix A , resulting in a matrix with the degree of each node. The subsequent left product with S^T impose another summation, whose result is a matrix composed by the sum of all elements of the blocks. Finally, the product by Γ^{-1} normalize the result by $\frac{1}{n}$. Formally we have,

$$AS = \begin{bmatrix} k^{11} & k^{12} & \dots & k^{1m} \\ k^{21} & k^{22} & \dots & k^{2m} \\ \vdots & \vdots & \ddots & \vdots \\ k^{m1} & k^{m2} & \dots & k^{mm} \end{bmatrix} \quad (39)$$

where $k^{ij} \in \mathbb{R}^{n \times 1}$ is a vector with the number of edges emanating from each node on layer i to layer j and $AS \in$

$\mathbb{R}^{nm \times m}$. Then,

$$S^T AS = \begin{bmatrix} \sum k^{11} & \sum k^{12} & \dots & \sum k^{1m} \\ \sum k^{21} & \sum k^{22} & \dots & \sum k^{2m} \\ \vdots & \vdots & \ddots & \vdots \\ \sum k^{m1} & \sum k^{m2} & \dots & \sum k^{mm} \end{bmatrix} \quad (40)$$

where $\sum k^{ij} \in \mathbb{R}$ are scalars with the number of edges that connect a node on layer i to a node on layer j . Finally, the product by Γ^{-1} introduce the average degree instead of the summation, producing the same results as Equation 24.

Appendix B: Eigenvalue crossing

Let us analyze the spectra of a simple setup: multiplex networks composed by l identical layers. Such class of networks provides insights about the spectral behavior as a function of $(\frac{\eta}{\lambda})$. Although they are not very realistic a priori, there are situations in which this representation is helpful: for instance, in the context of disease contagion, one might think of a multi-strain disease in which each strain propagates in a different layer allowing co-infection of the host population.

The adjacency tensor can be written as

$$\mathcal{R}_{\beta\delta}^{\alpha\tilde{\gamma}}(\lambda, \eta) = A_{\beta}^{\alpha}\delta_{\delta}^{\tilde{\gamma}} + \frac{\eta}{\lambda}\delta_{\beta}^{\alpha}K_{\delta}^{\tilde{\gamma}}, \quad (41)$$

where A_{β}^{α} is the 2-rank layer adjacency tensor, $K_{\tilde{\gamma}}^{\delta}$ is the adjacency tensor of the network of layers, which is a complete graph on the multiplex case, and δ_{β}^{α} is the Kronecker delta. Observe that it is the unfolding of a sum of two Kronecker products, $\bar{A} = I_m \otimes A + \frac{\eta}{\lambda}K_m \otimes I_n$, where I_n is the identity matrix of size n and K_m is the

adjacency matrix of the complete graph with m nodes. In this way, the eigenvalue problem can be written as

$$\mathcal{R}_{\beta\delta}^{\alpha\tilde{\gamma}}f_{\alpha\tilde{\gamma}} = A_{\beta}^{\alpha}\delta_{\delta}^{\tilde{\gamma}}f_{\alpha\tilde{\gamma}} + \frac{\eta}{\lambda}\delta_{\beta}^{\alpha}K_{\delta}^{\tilde{\gamma}}f_{\alpha\tilde{\gamma}}, \quad (42)$$

where the sum of the eigenvalues of A , Λ_i^l , and K , μ_i , are also eigenvalues of the adjacency tensor, hence $\mathcal{R}_{\beta\delta}^{\alpha\tilde{\gamma}}f_{\alpha\tilde{\gamma}} = (\Lambda_i^l + \frac{\eta}{\lambda}\mu_j)f_{\alpha\tilde{\gamma}}$, $i = 1, 2, \dots, n$ and $j = 1, 2, \dots, m$. Then,

$$\left(\Lambda_i^l + \frac{\eta}{\lambda}\mu_j\right) = \left(\Lambda_k^l + \frac{\eta}{\lambda}\mu_s\right). \quad (43)$$

The eigenvalues of the complete graph are $\mu_1 = m - 1$, and $\mu_i = -1$, $\forall i > 1$, yielding to

$$\frac{\eta}{\lambda} = \frac{\Lambda_k^l - \Lambda_i^l}{m}, \quad (44)$$

which imposes crossings on the eigenvalues of the adjacency tensor for identical layers, since $(\frac{\eta}{\lambda})$ is a continuous parameter.

-
- [1] R. Pastor-Satorras, C. Castellano, P. Van Mieghem, and A. Vespignani, *Rev. Mod. Phys.* **87**, 925 (2015).
- [2] R. M. Anderson and R. M. May, *Infectious Diseases of Humans Dynamics and Control* (Oxford University Press, 1992).
- [3] A. Barrat, M. Barthlemy, and A. Vespignani, *Dynamical processes on complex networks* (Cambridge University Press New York, NY, USA, 2008).
- [4] M. E. J. Newman, *SIAM REVIEW* **45**, 167 (2003).
- [5] S. Boccaletti, V. Latora, Y. Moreno, M. Chavez, and D. Hwang, *Physics Reports* **424**, 175 (2006).
- [6] L. Costa, F. Rodrigues, G. Traverso, and P. Boas, *Advances in Physics* **56**, 167 (2007), ISSN 0001-8732.
- [7] R. Pastor-Satorras and A. Vespignani, *Phys. Rev. Lett.* **86**, 3200 (2001).
- [8] M. Boguñá and R. Pastor-Satorras, *Phys. Rev. E* **66**, 047104 (2002).
- [9] M. Newman, *Networks: an introduction* (Oxford University Press, Inc., 2010).
- [10] Van Mieghem, P., *EPL* **97**, 48004 (2012).
- [11] S. C. Ferreira, C. Castellano, and R. Pastor-Satorras, *Phys. Rev. E* **86**, 041125 (2012).
- [12] Y. Wang, D. Chakrabarti, C. Wang, and C. Faloutsos, in *In SRDS* (2003), pp. 25–34.
- [13] P. V. Mieghem, J. Omic, and R. Kooij, *IEEE/ACM Trans. Netw.* **17**, 1 (2009).
- [14] S. Gómez, a. Arenas, J. Borge-Holthoefer, S. Meloni, and Y. Moreno, *EPL (Europhysics Letters)* **89**, 38009 (2010), ISSN 0295-5075.
- [15] P. Holme and J. Saramäki, *Physics Reports* **519**, 97 (2012), ISSN 0370-1573, temporal Networks.
- [16] E. Valdano, L. Ferreri, C. Poletto, and V. Colizza, *Phys. Rev. X* **5**, 021005 (2015).
- [17] M. E. J. Newman, *Phys. Rev. Lett.* **95**, 108701 (2005).
- [18] A. B. Pedersen and A. Fenton, *Trends in Ecology & Evolution* **22**, 133 (2007), ISSN 0169-5347.
- [19] H. J. W. D. A. V. Y. H. Pejman Rohani, *Understanding Host-Multipathogen Systems: Modeling the Interaction between Ecology and Immunology* (Princeton University Press, 2008), pp. 48–70.
- [20] P.-A. Noël, A. Allard, L. Hébert-Dufresne, V. Marceau, and L. J. Dubé, *Phys. Rev. E* **85**, 031118 (2012).
- [21] C. Poletto, M. Sandro, C. Vittoria, M. Yamir, and V. Alessandro, *PLoS Comput Biol* **9**, 1 (2013).
- [22] F. Darabi Sahneh and C. Scoglio, *Phys. Rev. E* **89**, 062817 (2014).
- [23] J. Sanz, C.-Y. Xia, S. Meloni, and Y. Moreno, *Phys. Rev. X* **4**, 041005 (2014).
- [24] S. Funk, E. Gilad, C. Watkins, and V. A. A. Jansen, *Proceedings of the National Academy of Sciences* **106**, 6872 (2009).
- [25] S. Funk, M. Salathé, and V. A. A. Jansen, *Journal of The Royal Society Interface* **7**, 1247 (2010), ISSN 1742-5689.
- [26] Meloni Sandro, Perra Nicola, Arenas Alex, Gómez Sergio, Moreno Yamir, and Vespignani Alessandro, *Scientific Reports* **1**, 62 (2011).
- [27] M. Kivelä, A. Arenas, M. Barthelemy, J. P. Gleeson, Y. Moreno, and M. A. Porter, *Journal of Complex Networks* **2**, 203 (2014).
- [28] E. Cozzo, R. A. Baños, S. Meloni, and Y. Moreno, *Phys. Rev. E* **88**, 050801 (2013).
- [29] M. De Domenico, A. Solé-Ribalta, E. Cozzo, M. Kivelä, Y. Moreno, M. A. Porter, S. Gómez, and A. Arenas, *Phys. Rev. X* **3**, 041022 (2013).
- [30] R. J. Sánchez-García, E. Cozzo, and Y. Moreno, *Phys. Rev. E* **89**, 052815 (2014).
- [31] A. V. Goltsev, S. N. Dorogovtsev, J. G. Oliveira, and J. F. F. Mendes, *Phys. Rev. Lett.* **109**, 128702 (2012).
- [32] E. Cator and P. Van Mieghem, *Phys. Rev. E* **89**, 052802 (2014).
- [33] E. Cozzo, G. F. Arruda, F. A. Rodrigues, and Y. Moreno, *Interconnected Networks* (Springer International Pub-

- lishing, 2016), chap. Multilayer Networks: Metrics and Spectral Properties, pp. 17–35.
- [34] A. S. Mata and S. C. Ferreira, *Phys. Rev. E* **91**, 012816 (2015).
- [35] J. Dormand and P. Prince, *Journal of Computational and Applied Mathematics* **6**, 19 (1980), ISSN 0377-0427.
- [36] F. Viger and M. Latapy, in *Proceedings of the 11th Annual International Conference on Computing and Combinatorics* (Springer-Verlag, Berlin, Heidelberg, 2005), COCOON'05, pp. 440–449.
- [37] F. Radicchi and A. Arenas, *Nature Physics* pp. 717–720 (2013).